*Desalination and Water Treatment*
www.deswater.com
doi: 10.1080/19443994.2014.902331

54 (2015) 2259–2269
May

Taylor & Francis
Taylor & Francis Group

# A rapid method for the removal of Methyl blue dye from wastewater by magnetic nanoparticles Mn-ferrites

Lei Zhang*, Yunyu Zhang, Lijun Yang, Xiaoqing Jiang, Qi Yang

*College of Chemistry, Liaoning University, Shenyang 110036, People's Republic of China, Tel. +86 24 62207809; Fax: +86 24 62202380; email: zhanglei63@126.com*

Received 2 September 2013; Accepted 9 February 2014

ABSTRACT

In this study, the adsorption processes of Methyl blue (MB) were investigated in the presence of magnetite nanoparticles ($MnFe_2O_4$). The MB removal reached close to 97% and MB adsorption had the highest capacity at pH 3.0–9.0. The MB adsorption reaction was found to be fast, and equilibrium was attained within 20.0 min following the pseudo-second-order model. The overall rate process was mainly controlled by the external mass transfer. The sorption data could be well interpreted by the Langmuir model with a maximum adsorption capacity of 148.04 mg $g^{-1}$ (298 K) for MB on $MnFe_2O_4$. Thermodynamics research showed that the adsorption was a spontaneous and exothermic process. The nano-$MnFe_2O_4$ could be separated from wastewater under an external magnetic field and reused for eight times without obvious significant loss of its adsorption activity for MB. With the advantages of rapid adsorption process and high-efficient magnetic separation, the $MnFe_2O_4$ could gain a promising application in wastewater treatment.

*Keywords:* Adsorption; Magnetic nanoparticles; Methyl blue; Mn-Ferrites

## 1. Introduction

Dyes are widely used in textiles, paper, plastics, leather, food, and cosmetic industries. The color of the untreated effluent into the receiving water body not only causes damage to aquatic life, but also to human beings by mutagenic or carcinogenic effects [1]. Most of the organic dye compounds ordinarily contain benzene and naphthalene rings, and they cannot be decomposed easily by conventional biological and chemical methods. Consequently, there is considerable need to treat colored effluents prior to their discharge into receiving waters to prevent environmental pollution in the aquatic ecosystems.

Methyl blue (MB) is one of the triphenylmethane acid dyes. Due to its complex aromatic structures and good water solubility, MB dye resist fade when exposed to light, water, and many chemicals, and therefore it was difficult to be decolorized once MB was released into the aquatic environment.

The magnetic separation method has attracted much attention because of high separation rate using a simple magnetic process. Several reports have been published on the use of various types of magnetic particles for the removal of dyes, such as $Fe_{3-x}La_xO_4$ [2], activated carbon/$Fe_2O_3$ [3], activated carbon/$CoFe_2O_4$ [4], and montmorillonite/$CoFe_2O_4$ magnetic composite [5]. In particular, the ferrites with spinel structure exhibit interesting magnetic properties that are potential adsorbents for the

*Corresponding author.

removal of contaminations from wastewater [6]. Recently, the exploitation of $ZnFe_2O_4$ [7], $CoFe_2O_4$ [8], $NiFe_2O_4$ [9], and $MnFe_2O_4$ [10] in water treatment has been studied, which exhibited the excellent adsorptive properties capable of highly effective recovery by magnetic separation technique. Nano-sized magnetic particles are considered as potential adsorbents for aqueous pollutants due to their high surface area and removal capacity. Several reports have been published on the use of various types of magnetic nanoparticles for removal and separation of dyes [11–16].

To the best of our knowledge, little work has been done on the preparation of nano-$MnFe_2O_4$ for the removal of MB. Therefore, very little is known about the kinetic and thermodynamic characteristics of MB adsorption on nano-$MnFe_2O_4$.

In this paper, nano-$MnFe_2O_4$ as a sorbent was used for the removal of MB from solutions; the adsorption behavior of MB on $MnFe_2O_4$ was investigated in detail. The best conditions for the removal of MB were studied and optimized. The object of the experiment was not only to know the adsorption mechanism between MB and $MnFe_2O_4$, but also to guide the application of the magnetic adsorbents in the removal of dyes from wastewater.

## 2. Experimental section

### 2.1. Chemicals

MB (CAS: 2893-56-4) chemical was bought from Sinopharm Chemical Reagent Co., Ltd, whose concentration was analyzed by colorimetric assay at 590 nm. An accurately weighed quantity of the dye was dissolved in deionized water to prepare the stock solution (1.0 g $L^{-1}$). All other chemicals used in this experiment were of analytical grade. Deionized water was used throughout the experiment.

### 2.2. Preparation of $MnFe_2O_4$

Adsorbent: $MnFe_2O_4$ was synthesized through a co-precipitation method. The preparation of $MnFe_2O_4$ was performed as follows: some $MnCl_2$ and $FeCl_3$ salts with a molar ratio of 1:2 were dissolved in 200 mL of deionized water. Under vigorous magnetic stirring and continuous $N_2$-purging, 2.5 mol $L^{-1}$ NaOH was added dropwise to the solution until its pH was around 11. The precipitate was filtered, washed with deionized water, and dried in a muffle furnace at 110°C for 24 h. Then as-prepared sample $MnFe_2O_4$ was calcined at 500°C for 2 h.

### 2.3. Characterization of $MnFe_2O_4$

Measurement of BET surface area and pore distribution were performed using $N_2$ adsorption/desorption isotherms on a Micromeritics (Norcross, GA). The X-ray diffraction (XRD) patterns of $MnFe_2O_4$ powder were recorded on Siemens D5000 Diffractometer (Germany). The FT-IR spectra of $MnFe_2O_4$ were measured using the FT-IR 5700 (Nicolet Company, USA). Vibrating sample magnetometer (VSM, Lakeshore 7407) was used to measure the magnetic prosperities of $MnFe_2O_4$. The morphology of $MnFe_2O_4$ was determined by scanning electron microscope (SEM, FEI Inspect, USA) operated at 200 kV. A Malvern Zetasizer Nano-ZS particle analyzer (Malvern, UK) was used to determine the $\zeta$ potential of the sorbents. The pH of MB solution was measured by S-3C model pH meter (China). UV–vis-NIR Cary 5000 (Varian, USA) was used to investigate the removal efficiency of the dye.

### 2.4. Adsorption procedure

Duplicate and triplicate samples were used for the experiments of adsorption isotherm and conditions (pH and ion strength), respectively. The pH values of the solution were adjusted in the range of 3.0–9.0 with dilute HCl and NaOH.

Batch adsorption experiments were conducted using 50 mL flasks containing 70.0 mg $MnFe_2O_4$ and 25 mL of 30.0 mg $L^{-1}$ MB solution. After stirring at a constant rate at 293 K for 30.0 min, the solid/liquid phases were separated using a magnet. Then the concentration of MB was determined by UV–vis spectrophotometry.

Kinetic experiments were performed using a series of 50 mL flasks containing 70.0 mg $MnFe_2O_4$ and 25 mL of 30.0 mg $L^{-1}$ MB solution in a temperature range of 286–313 K. On regular time intervals, suitable aliquots were taken, whereupon the MB concentration was determined. The rate constants were calculated using the conventional rate expression.

Adsorption isotherm studies were carried out with different initial concentrations of MB ranging from 100.0 to 900.0 mg $L^{-1}$ (25 mL sample volume), the amount of adsorbent was kept constant (70.0 mg), and the experimental temperatures were controlled at 286, 298, and 313 K, respectively. The thermodynamic parameters for the adsorption process were determined at each temperature.

### 2.5. Regeneration experiments

The regeneration of MB-adsorbed $MnFe_2O_4$ was carried out by thermal degradation test. After

magnetic separation, $MnFe_2O_4$ was collected and dried at 100℃, then placed into a muffle furnace and heated at 400℃ for 2 h. After the thermal reaction, the regenerated adsorbent was washed with 10 mL NaOH solution for further test.

### 2.6. Water samples

Water samples were collected from river water, drinking water, effluents, and synthetic water. The effluents used in this study were collected from a municipal wastewater treatment plant (Shenyang, China). The samples were stored at 4℃ in polyethylene (LDPE) bottles.

The synthetic water samples spiked with 30 mg $L^{-1}$ MB dye were used in the experiments. A total of 1 mM each of $Fe^{3+}$, $Ni^{2+}$, $Cu^{2+}$, $Zn^{2+}$, $Pb^{2+}$, $Ac^{-}$, $CO_3^{2-}$, $SO_4^{2-}$, $SO_3^{2-}$ and $PO_4^{3-}$ ions were separately added into the synthetic water mentioned above.

## 3. Results and discussion

### 3.1. Characteristics of $MnFe_2O_4$

The morphology of $MnFe_2O_4$ was studied by SEM (Fig. 1(a)). The SEM image of $MnFe_2O_4$ showed that the main particle size was in the range of 86–94 nm. Fig. 1(b) presented the nitrogen adsorption–desorption isotherms and Barret–Joyner–Halenda pore size distribution curve (inset) of the $MnFe_2O_4$. The BET surface area, pore volume, and average pore diameter of $MnFe_2O_4$ were determined to be 78.52 $m^2 g^{-1}$, 0.08 $cm^3 g^{-1}$, and 16 nm, respectively. Fig. 1(c) showed the XRD patterns of $MnFe_2O_4$. The result indicated that the crystallinity of $MnFe_2O_4$ phase increased with an increase of calcination temperature. The diffraction patterns can be indexed with the cubic spinel structure.

The magnetic properties of the $MnFe_2O_4$ were analyzed at room temperature VSM with an applied field

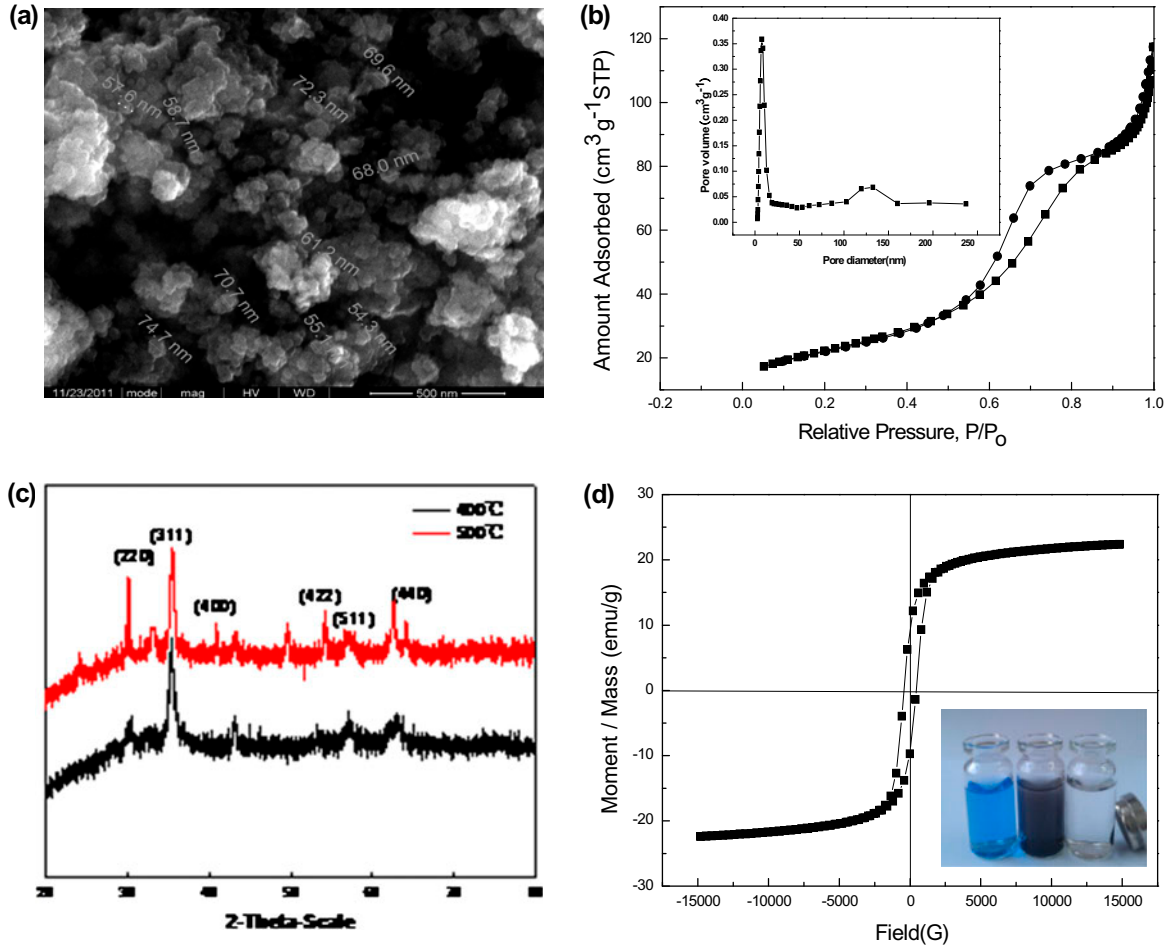


Fig. 1. (a) SEM image of $MnFe_2O_4$; (b) the particle diameter distributions of $MnFe_2O_4$; (c) XRD spectra of $MnFe_2O_4$; and (d) VSM magnetization curves of $MnFe_2O_4$ (inset: photo of magnetic separation).

of $-15.0 \le H \le 15.0$ kOe (Fig. 1(d)). The value of saturation magnetization (Ms) was about 22.38 emu $g^{-1}$, the remnant magnetization (Mr) and coercivity field were 3.3 emu $g^{-1}$ and 437.2 Oe, respectively. It could also be seen from Fig. 1(d) (the inset showed the photo of magnetic separation), that $MnFe_2O_4$ could be separated from solution under an external magnetic field.

### 3.2. Influence of $MnFe_2O_4$ dosage on adsorption

A detailed study on the adsorption process was performed by varying the sorbent amount and sorption time. Twenty-five milliliters of 30.0 mg $L^{-1}$ MB solutions was applied to test the sorption behavior at different conditions. It was found that the adsorption percentages increased with the increase in the dose of $MnFe_2O_4$, and when the amount exceeded 70.0 mg, further increase in the dose had negligible effect on the sorption. Therefore, 70.0 mg of $MnFe_2O_4$ was selected for the adsorption of MB, and the systems could reach equilibrium around 15.0 min.

### 3.3. Effect of pH and ionic Strength

To evaluate the pH of solution, 70.0 mg of $MnFe_2O_4$ was added to 25 mL of 30.0 mg $L^{-1}$ MB solutions. The effect of pH of solution on MB adsorption is shown in Fig. 2(a). The adsorption maxima generally occurred between pH 3.0–9.0. In general, the natural pH of dye solution was close to 5.5. In this work, the dye solution was used directly without any pH adjustment with HCl or NaOH.

MB adsorption data under two ionic strengths (0.02 and 0.2 mol $L^{-1}$ as NaCl and the initial MB concentrations 30.0 mg $L^{-1}$) are given in Fig. 2(b). In the entire experimental pH range, MB adsorption data under two ionic strengths overlapped, indicating that the ionic strength did not impact the adsorption of MB onto $MnFe_2O_4$.

### 3.4. Mechanistic aspects

The pH variation can not only affect the protonation–deprotonation transition of $MnFe_2O_4$, but also result in a change in chemical speciation for ionizable organic compounds. The values of zeta potential of $MnFe_2O_4$ suspensions were determined under various pH values, and the point of zero charge of $MnFe_2O_4$ was found to be about 6.6 (Fig. 2(c)). At pH < 6.6, the $MnFe_2O_4$ surface carries positive charge, while at pH > 6.6, the $MnFe_2O_4$ surface is negatively charged. However, as could be seen from Fig. 2(a), there was no remarkable effect on the adsorption of MB on

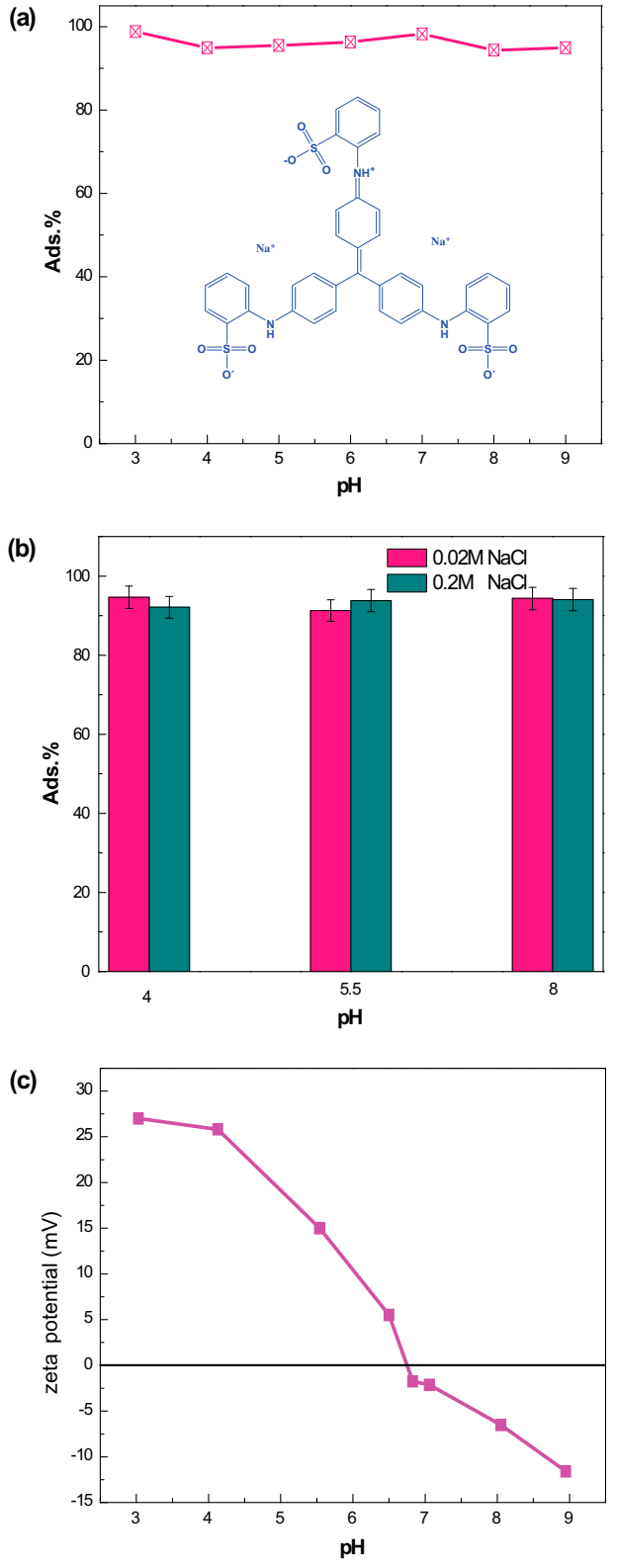


Fig. 2. (a) Effect of pH; (b) effect of ionic strength, and (c) zeta potential of $MnFe_2O_4$ under various pH.

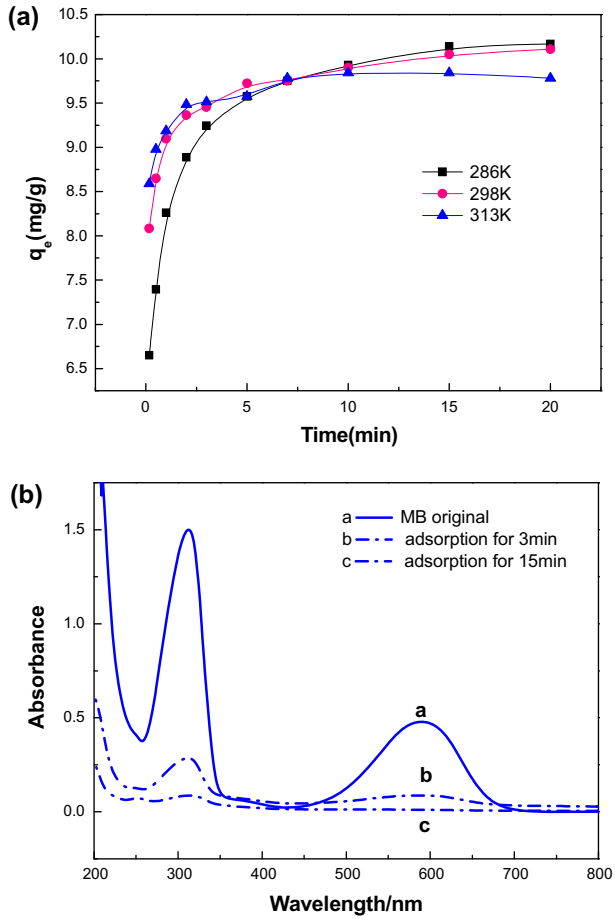


Fig. 3. (a) Kinetic curves of MB removal by $MnFe_2O_4$ and (b) The UV absorption spectrogram at different time.

$MnFe_2O_4$ with an increase of pH from 3.0 to 9.0. This result indicated that the sorption process of MB was not mainly controlled by the electrostatic interaction. Furthermore, the ionic strength test also confirmed that the surface electrostatic effect had no influence on the overall adsorption of MB on $MnFe_2O_4$.

H-bonds interaction may be formed between the –NH and = $NH^+$ groups of MB and the –OH groups of $MnFe_2O_4$. The overall adsorption mechanism was mainly controlled by the strength of hydrogen bonds.

### 3.5. Adsorption kinetic model

The influence of contact time on the removal of MB by $MnFe_2O_4$ are present in Fig. 3. The adsorption could reach equilibrium in less than 20 min, and the short adsorption equilibrium time indicated that it was a very fast adsorption process.

The rate at which the MB is removed from solution onto an adsorbent surface is an important factor for designing treatment plants. In order to investigate the adsorption processes of MB on $MnFe_2O_4$, the two kinetic models were used, including pseudo-first-order and pseudo-second-order models [17].

#### 3.5.1. Pseudo-first-order model

$$\lg(q_e - q_t) = \lg q_e - \frac{k_1 t}{2.303} \quad (1)$$

where $q_e$ and $q_t$ are the amounts of MB adsorbed on the sorbent (mg $g^{-1}$) at equilibrium and at time $t$, respectively, and $k_1$ is the rate constant of the first-order adsorption ($min^{-1}$). The values of $k_1$ for MB adsorption on $MnFe_2O_4$ were calculated from the plot of $\lg(q_e - q_t)$ against $t$.

Kinetic parameters of the model are present in Table 1. The values of $r_1$ for MB adsorption onto $MnFe_2O_4$ were larger than 0.95. However, the calculated values of adsorption capacity at equilibrium ($q_e$) were far different from the actual amount adsorbed at equilibrium, suggesting that the pseudo-first-order model is not an appropriate one.

#### 3.5.2. Pseudo-second-order model

$$\frac{t}{q_t} = \frac{1}{k_2 q_e^2} + \frac{t}{q_e} \quad (2)$$

where $k_2$ is the rate constant of the second-order adsorption (g $mg^{-1}$ $min^{-1}$). The straight-line plots of $t/q_t$ vs. $t$ have been tested to obtain rate parameters.

As shown in Table 1, the data were then fitted with the pseudo-second-order equation, the values of

Table 1
Kinetic parameters for the removal MB by $MnFe_2O_4$

| | | Pseudo-first-order model | | | Pseudo-second-order model | | |
|---|---|---|---|---|---|---|---|
| Dye | $T/K$ | $k_1$ ($min^{-1}$) | $q_1$ (mg $g^{-1}$) | $r_1$ | $k_2$ (g $mg^{-1}$ $min^{-1}$) | $q_2$ (mg $g^{-1}$) | $r_2$ |
| MB | 286 | 0.274 | 2.638 | 0.976 | 0.365 | 10.273 | 0.999 |
| | 298 | 0.237 | 1.390 | 0.965 | 0.627 | 10.143 | 0.999 |
| | 313 | 0.377 | 0.942 | 0.958 | 1.621 | 9.842 | 0.999 |

$r_2$ are larger than 0.99 which showed that the pseudo-second-order model provided better description on the data obtained when compared to the pseudo-first-order model. Moreover, the calculated values of adsorption equilibrium were comparable to the actual amount of adsorption equilibrium.

### 3.6. Adsorption rate-controlling mechanism

In adsorption process, only intra-particle diffusion and external mass transfer play important roles in rate determination. To evaluate the relative importance of the two steps, time-course MB sorption data were processed using the intra-particle diffusion [18] and the external mass transfer models.

#### 3.6.1. Weber–Morris intra-particle diffusion model

$$q_t = K_d t^{1/2} + I \tag{3}$$

where $q_t$ is the amount of MB adsorbed at time $t$, $K_d$ is the rate constant for intra-particle diffusion. Values of $I$ give an idea about the thickness of the boundary layer, i.e. the larger the intercept, the greater the boundary layer effect will be [19,20]. The plots of $q_t$ vs. $t^{1/2}$ for the sorption of MB are shown in Fig. 4(a). Piecewise linear regression of data showed that $q_t$ vs. $t^{1/2}$ plots had two distinct regions. The first linear portions included the sorption period of 0.0–3.0 min, which represented external mass transfer and binding of MB by those active sites distributed onto the outer surface of $MnFe_2O_4$. The second linear portions included the sorption period of 3.0–20.0 min, representing intra-particle diffusion and binding of MB by active sites distributed to macropores, mesopores, and micropores of $MnFe_2O_4$ [21,22]. Generally, the adsorption rate was controlled by the outer diffusion or the inner diffusion or both. Nonetheless, $I$ was $\neq 0$ in the test conditions (Fig. 4(a)), thereby suggesting that the intra-particle diffusion was not only the rate-limiting step, and that the external mass transfer had also played an important role in MB sorption by $MnFe_2O_4$.

#### 3.6.2. External mass transfer model

$$\left[\frac{d(C_t/C_i)}{dt}\right]_{t=0} = -\beta S \tag{4}$$

where $C_i$ and $C_t$ represent the concentrations of MB in the beginning and at time $t$ (mg $L^{-1}$), respectively; $\beta$ is the external mass transfer coefficient (cm $min^{-1}$); $S$ is the specific surface of $MnFe_2O_4$ for external mass

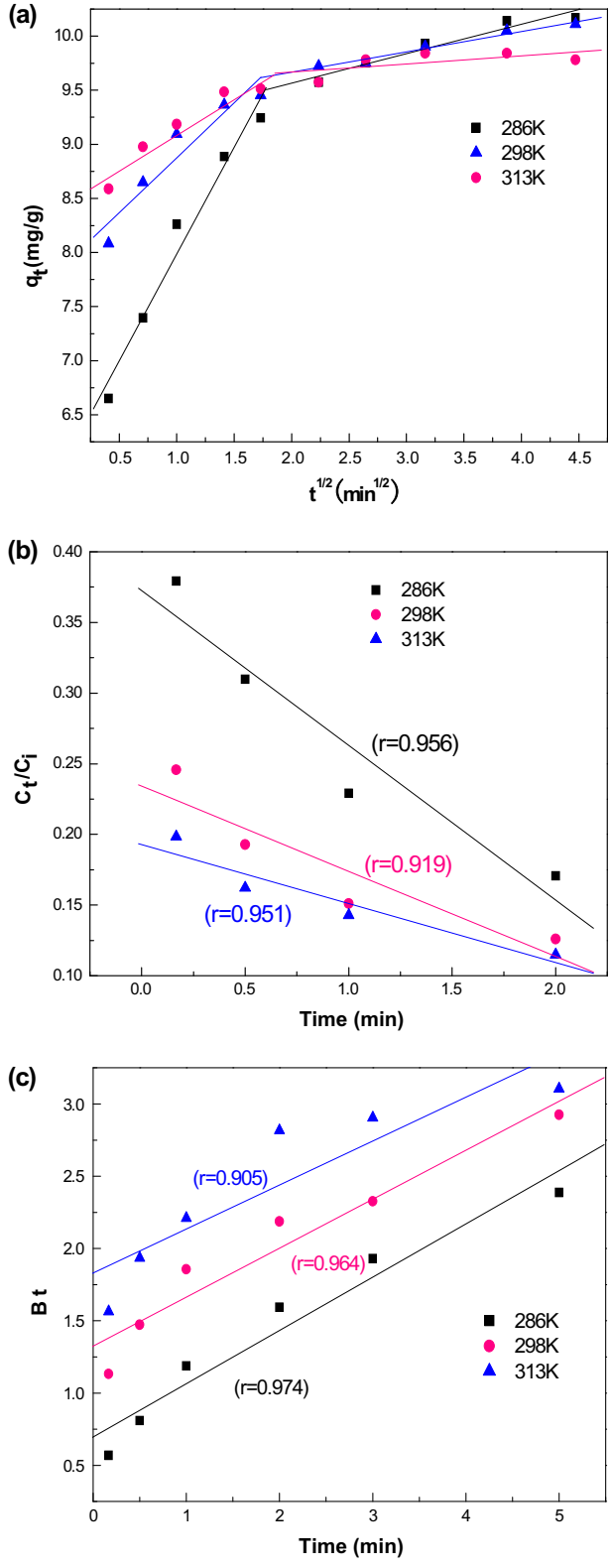


Fig. 4. (a) Weber–Morris plots, (b) external mass transfer plots, and (c) Boyd plots for the adsorption of MB on $MnFe_2O_4$.

transfer ($cm^{-1}$), with the assumption $C_t = C_i$ at $t = 0$. Then $\beta S$ values were calculated by the slope of the plot of $C_t/C_i$ vs. time $t$ (Fig. 4(b)) and the initial rate found to be 0.226, 0.160, and 0.079 $min^{-1}$ at 286, 298, and 313 K, respectively. High regression coefficients showed that MB adsorption data could be interpreted by the external mass transfer model.

The above discussion made it amply clear that both intra-particle and external mass transfer processes played important roles in the sorption of MB. However, it was unclear as to which one exerted a greater influence on the rate of MB sorption. This point was resolved using the Boyd model.

#### 3.6.3. Boyd model [23]

$$Bt = -\ln(1 - F) - 0.4977 \quad (5)$$

where $F = q_t/q_e$; $q_t$ and $q_e$ are the amounts of MB adsorbed on $MnFe_2O_4$ (mg $g^{-1}$) at time $t$ (min) and at equilibrium time (min), respectively; $Bt$ values were calculated for MB sorption at different time periods ($q_t$). Boyd plots for the sorption of MB at three different temperatures are present in Fig. 4(c). However, the straight lines for MB did not pass through the origin. This indicated that the adsorption of MB on the $MnFe_2O_4$ was mainly governed by the external mass transport at temperature in the range 286–313 K [21].

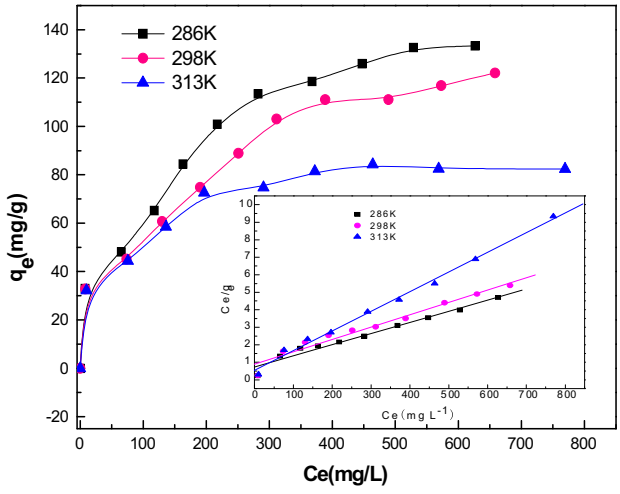


Fig. 5. Adsorption isotherm for MB at different temperatures (286, 298, and 313 K).

### 3.7. Adsorption isotherms

Analysis of equilibrium data is important for evaluating adsorption properties of $MnFe_2O_4$ adsorbent. The adsorption capacity of MB on $MnFe_2O_4$ at equilibrium as a function of the equilibrium concentration of MB is depicted in Fig. 5. An increased adsorption was observed for MB until the saturation was attained. In order to investigate the adsorption isotherm of MB on $MnFe_2O_4$, the Langmuir and Freundlich isotherm models were used.

Langmuir model:

$$\frac{C_e}{q_e} = \frac{C_e}{q_m} + \frac{1}{bq_m} \quad (6)$$

Freundlich model:

$$\lg q_e = \lg K_F + \frac{1}{n}\lg c_e \quad (7)$$

where $q_m$ is the maximum monolayer adsorption (mg $g^{-1}$), $C_e$ is the equilibrium concentration of MB (mg $L^{-1}$), $q_e$ is the amount of MB adsorbed per unit weight of $MnFe_2O_4$ at equilibrium (mg $g^{-1}$), and $b$ is the Langmuir constant related to the affinity of binding sites (L $mg^{-1}$). $K_F$ and $n$ are Freundlich constants indicating the sorption capacity and intensity, respectively.

The isothermal constants and the linear regression coefficients extracted from the experimental data are present in Table 2. It was found that the adsorption of MB on $MnFe_2O_4$ correlated well with the Langmuir equation when compared to the Freundlich equation under the studied concentration range. The maximum adsorption capacity of MB on $MnFe_2O_4$ was 157.48,

Table 2
Langmuir, Freundlich, and D–R constants of the adsorption of MB on $MnFe_2O_4$

| | Langmuir | | | Freundlich | | | D–R | | |
|---|---|---|---|---|---|---|---|---|---|
| $T$/K | $b$ L $mg^{-1}$ | $q_m$ mg $g^{-1}$ | $r_1$ | $n$ | $k_F$ | $r_2$ | $q_m$ mg $g^{-1}$ | $E$ kJ $mol^{-1}$ | $r_3$ |
| 286 | 0.009 | 157.480 | 0.984 | 2.819 | 13.926 | 0.971 | 131.197 | 0.017 | 0.986 |
| 298 | 0.008 | 142.045 | 0.981 | 3.023 | 13.967 | 0.963 | 117.214 | 0.016 | 0.963 |
| 313 | 0.021 | 88.970 | 0.997 | 4.067 | 17.767 | 0.970 | 84.453 | 0.022 | 0.982 |

Table 3
Maximum adsorption capacities for the adsorption of MB onto various adsorbents

| Absorbent | Adsorption capacity (mg $g^{-1}$) | Reference |
|---|---|---|
| $MnFe_2O_4$ | 148.04 | This work |
| Natural chitosan membranes | 46.23 | [24] |
| Magnetic chitosan | 60.4 | [24] |
| Graphene oxide | 43.5 | [24] |
| Magnetic chitosan and graphene oxide | 98.52 | [24] |
| Activated charcoal | 25.25 | [25] |
| Graphene | 50 | [26] |

148.04, and 88.97 mg $g^{-1}$ at 286, 298, and 313 K, respectively.

Table 3 represented the maximum adsorption capacities of $MnFe_2O_4$ onto various adsorbents. The comparison revealed that $MnFe_2O_4$ has higher adsorption capacity than other reported adsorbents.

Finally, the Dubinin–Radushkevich (D–R) isotherm was also tested in its linearized form:

$$\ln q_e = \ln q_m - K\varepsilon^2 \tag{8}$$

where $q_e$ and $q_m$ are the amounts of MB adsorbed at equilibrium time and at maximum monolayer, respectively, $K$ is the parameter related to the adsorption energy. $\varepsilon$ is the adsorption potential. The Polanyi potential varies with the concentration according to:

$$\varepsilon = RT \ln\left(1 + \frac{1}{C_e}\right) \tag{9}$$

where $R$ is the ideal gas constant and $T$ is temperature (K). A linear regression correlation was obtained by plotting $\ln q_e$ vs. $\varepsilon^2$ (shown in Table 2), indicating that MB adsorption also obeyed the D–R equation. The adsorption energy for MB adsorption can be calculated by:

$$E = (-2K)^{-1/2} \tag{10}$$

The values of the adsorption energy were evaluated as 0.017, 0.016, and 0.022 kJ $mol^{-1}$ at 286, 298, and 313 K, respectively, indicating that the values lie within the energy range of physical adsorption, i.e. <8 kJ $mol^{-1}$ [27].

### 3.8. Thermodynamic studies

The thermodynamic parameters provide in-depth information regarding the inherent energetic changes associated with adsorption; therefore, they should be properly evaluated. The sorption behaviors of different concentrations of MB onto $MnFe_2O_4$ were critically investigated at 286, 298, and 313 K, respectively. Thermodynamic parameters were calculated from following equations:

$$\Delta G^0 = -RT \ln K_c \tag{11}$$

where $T$ is temperature (K) and $K_c$ is the distribution coefficient. Gibbs free energy change of adsorption ($\Delta G^0$) was calculated using ln $K_c$ values for different temperatures. The $K_c$ value was calculated using the following equation:

$$K_c = \frac{q_e}{C_e} \tag{12}$$

where $C_e$ is the equilibrium concentration of MB and $q_e$ is the amount of MB adsorbed per unit weight of $MnFe_2O_4$ at equilibrium concentration (mg $g^{-1}$).

The enthalpy change ($\Delta H^0$) and entropy change ($\Delta S^0$) of adsorption were estimated from the following equation:

$$\ln K_c = \frac{\Delta S^0}{R} - \frac{\Delta H^0}{RT} \tag{13}$$

According to Eq. (13), $\Delta H^0$ and $\Delta S^0$ parameters can be calculated from the slope and intercept of the plot of ln $K_c$ vs. $1/T$, respectively.

The negative values of $\Delta H^0$ (−7.834 kJ $mol^{-1}$) and $\Delta G^0$ (−3.456, −3.432, and −3.050 kJ $mol^{-1}$ at 268 K, 298 K, and 333 K, respectively) showed the exothermic and spontaneous nature of the sorption process.

### 3.9. Effect of various ions on adsorption

Since industrial wastewater is always contained with various additives, such as inorganic salts, it is important to study the effect of these ions on the adsorption property of dyes. The adsorption of MB in

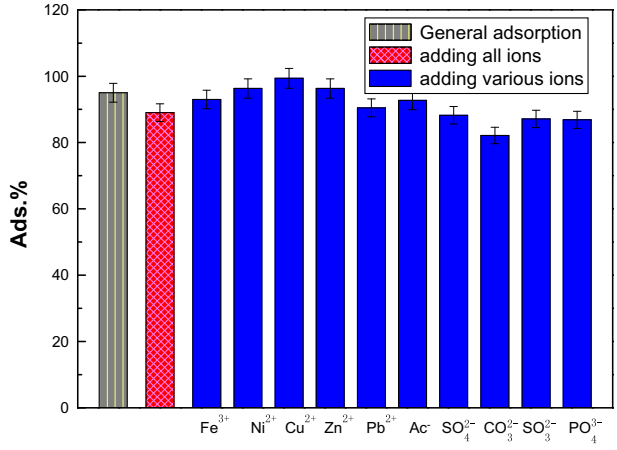


Fig. 6. Effect of the major cations and anions on adsorption.

the presence of anions and cations was carried out. The concentrations of all these ions in solution were kept at $1 \times 10^{-3}$ mol $L^{-1}$ in each case. It is shown in Fig. 6, that the coexisting ions almost had no negative effect on the MB adsorption of $MnFe_2O_4$, which also decided the possible practical application of $MnFe_2O_4$.

### 3.10. Reusability of $MnFe_2O_4$

The regeneration of the adsorbent is important to reduce the cost of the adsorption process. The thermal decomposition method is a feasible approach to regenerate the dye-loaded adsorbents. The temperature and time required to achieve good regeneration efficiency were 400°C and 1 h, respectively. In order to evaluate the stability of regenerated adsorbent, repeated application of $MnFe_2O_4$ experiments have been performed, and their removal efficiencies are shown in Fig. 7(a). It was stable for up to eight adsorption cycles without obvious decrease in the removal efficiency for dyes.

In the FT-IR spectra of $MnFe_2O_4$ Fig. 7(b), after adsorption, the $MnFe_2O_4$ showed some apparent characteristic bands of MB, while $MnFe_2O_4$ did not display these apparent characteristic bands before adsorption. It could also be seen from Fig. 7(b), that the main functional groups of MB disappeared after thermal decomposition. After the eighth recycle, FT-IR of $MnFe_2O_4$ did not show evident change when compared to that of the first recycle. The experimental results indicated that the $MnFe_2O_4$ has an excellent regeneration/reuseability.

### 3.11. Potential use of $MnFe_2O_4$ to treat MB-containing wastewaters

The removal efficiencies of MB in different water samples using $MnFe_2O_4$ were studied. Removal

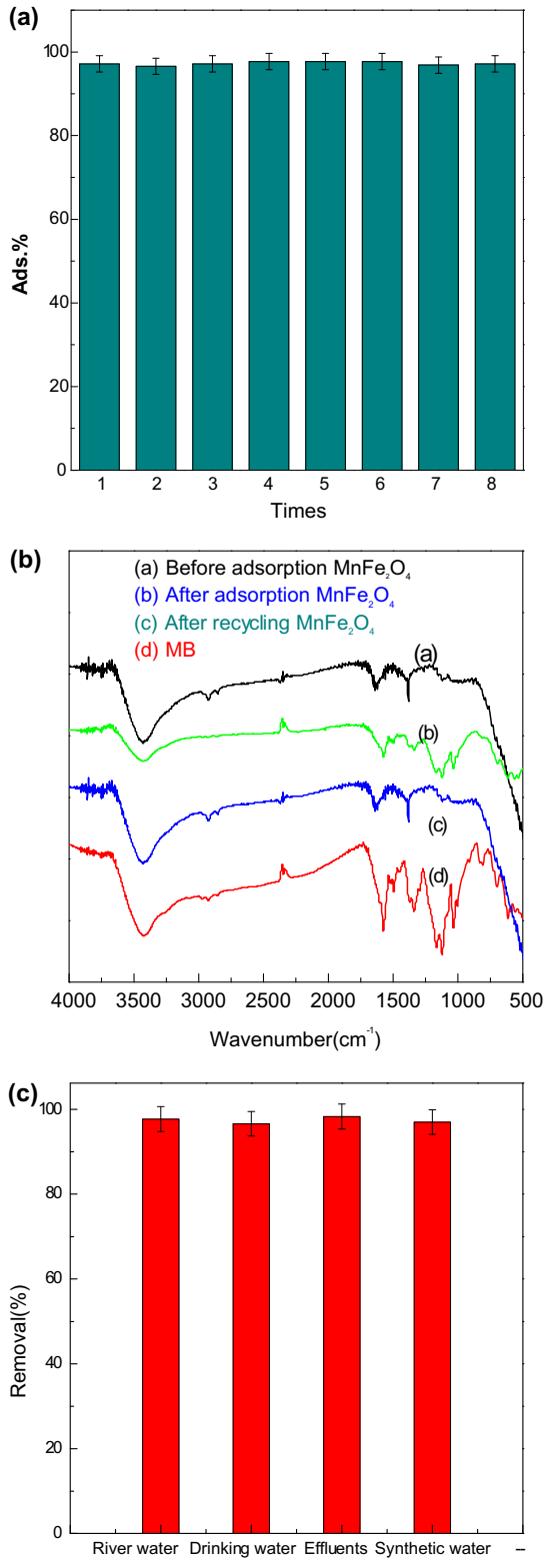


Fig. 7. (a) Times of $MnFe_2O_4$ powder recycling use; (b) the IR spectrogram of $MnFe_2O_4$ and MB; and (c) removal efficiency of $MgFe_2O_4$ towards different kinds of water (25 mL of 30 mg $L^{-1}$ MB, temperature 25 ± 2°C).

efficiencies of MB from different water sources (river water, drinking water, effluents, and synthetic water) were ranged from 96 to 98% (Fig. 7(c)). For each 25 mL 30 mg $L^{-1}$ MB sample, the removal efficiencies were up to 96%, suggesting that the $MnFe_2O_4$ has a strong anti-interference ability in different water environments.

## 4. Conclusion

Overall, this study demonstrated high removal efficiencies of MB from wastewater with broad pH values (3.0−9.0) using nano-$MnFe_2O_4$. Changes of ionic strength had a negligible effect on adsorptive characteristics. The common ion competitive influence on MB adsorption could be ignored. The thermodynamic parameters implied that the adsorption was a spontaneous and exothermic process. Adsorption mechanism study revealed that the processes were complex and the overall rate processes appeared to be influenced by both the intra-particle diffusion and external mass transfer, but mainly governed by the external mass transfer. Besides, the $MnFe_2O_4$ can be reused at least eight times without obvious decrease in the removal efficiency. The test results of kinetic and thermodynamic studies would be useful for the design of wastewater treatment plants for the dyes removal.

## Acknowledgments

This project was supported by the National Nature Science Foundation of China (NSFC51178212), Science Foundation of the Education Department of Liaoning Province (No. L2011007), Liaoning Provincial Department of education innovation team projects (LT2012001), the Shenyang Science and Technology Plan (F12-277-1-69), and the Foundation of 211 project for Innovative Talent Training, Liaoning University. The authors also thank their colleagues and other students who participated in this work.

## References

[1] K. Kadirvelu, M. Kavipriya, C. Karthika, M. Radhika, N. Vennilamani, S. Pattabhi, Utilization of various agricultural wastes for activated carbon preparation and application for the removal of dyes and metal ions from aqueous solutions, Bioresour. Technol. 87 (2003) 129–132.

[2] L.X. Wang, J.C. Li, Y.Q. Wang, L.J. Zhao, Preparation of nanocrystalline $Fe_{3-x}La_xO_4$ ferrite and their adsorption capability for Congo red, J. Hazard. Mater. 196 (2011) 342–349.

[3] S. Qu, F. Huang, S. Yu, G. Chen, J. Kong, Magnetic removal of dyes from aqueous solution using multi-walled carbon nanotubes filled with $Fe_2O_3$ particles, J. Hazard. Mater. 160 (2008) 643–647.

[4] L.H. Ai, H.Y. Huang, Z.L. Chen, X. Wei, J. Jiang, Activated carbon/$CoFe_2O_4$ composites: Facile synthesis, magnetic performance and their potential application for the removal of malachite green from water, Chem. Eng. J. 156 (2010) 243–249.

[5] L.H. Ai, Y. Zhou, J. Jiang, Removal of methylene blue from aqueous solution by montmorillonite/$CoFe_2O_4$ composite with magnetic separation performance, Desalination 266 (2011) 72–77.

[6] N. Bao, L. Shen, Y. Wang, P. Padhan, A. Gupta, A facile thermolysis route to monodisperse ferrite nanocrystals, J. Am. Chem. Soc. 129 (2007) 12374–12375.

[7] L. Zhang, Degradation of malachite green solution using combined microwave and $ZnFe_2O_4$ powder, Water Sci. Technol. 60 (2009) 2563–2569.

[8] L. Zhang, M.M. Su, X.J. Guo, Studies on the treatment of brilliant green solution by combination microwave induced oxidation with $CoFe_2O_4$, Sep. Purif. Technol. 62 (2008) 458–463.

[9] X.Y. Hou, J. Feng, X.H. Liu, Y.M. Ren, Z.J. Fan, T. Wei, J. Meng, M.L. Zhang, Synthesis of 3D porous ferromagnetic $NiFe_2O_4$ and using as novel adsorbent to treat wastewater, J. Colloid Interface Sci. 362 (2011) 477–485.

[10] X.Y. Hou, J. Feng, X.H. Liu, Y.M. Ren, Z.J. Fan, M.L. Zhang, Magnetic and highrate adsorption properties of porous $Mn_{1-x}Zn_xFe_2O_4$ $(0 \le x \le 0.8)$ adsorbents, J. Colloid Interface Sci. 353 (2011) 524–529.

[11] B. Zargar, H. Parham, A. Hatamie, Fast removal and recovery of amaranth by modified iron oxide magnetic nanoparticles, Chemosphere 76 (2009) 554–557.

[12] M. Liao, K. Wu, D. Chen, Fast removal of basic dyes by a novel magnetic nano-adsorbent, Chem. Lett. 32 (2003) 488–489.

[13] S. Mak, D. Chen, Fast adsorption of methylene blue on polyacrylic acid-bound iron oxide magnetic nanoparticles, Dye Pig. 61 (2004) 93–98.

[14] Y. Chang, D. Chen, Adsorption kinetics and thermodynamics of acid dyes on a carboxymethylated chitosan-conjugated magnetic nano-adsorbent, Macromol. Biosci. 5 (2005) 254–261.

[15] A. Mittal, L. Kurup, V.K. Gupta, Use of waste materials—bottom ash and De-Oiled Soya, as potential adsorbents for the removal of amaranth from aqueous solutions, J. Hazard. Mater. 117 (2005) 171–178.

[16] V. Rocher, J.M. Siaugue, V. Cabuil, A. Bee, Removal of organic dyes by magnetic alginate beads, Water Res. 42 (2008) 1290–1298.

[17] S. Azizian, Kinetic models of sorption: A theoretical analysis, J. Colloid Interface Sci. 276 (2004) 47–52.

[18] W.J. Weber, J.C. Morris, Kinetics of adsorption on carbon solution, J. Sanit. Eng. Div. Am. Soc. Civil Eng. 89 (1963) 31–60.

[19] V.S. Mane, I.D. Deo Mall, V.C. Chandra Srivastava, Kinetic and equilibrium isotherm studies for the adsorptive removal of brilliant green dye from aqueous solution by rice husk ash, J. Environ. Manage. 84 (2007) 390–400.

[20] A. Khenifi, B. Zohra, B. Kahina, H. Houari, D. Zoubir, Removal of 2,4-DCP from wastewater by CTAB/bentonite using one-step and two-step methods: A comparative study, Chem. Eng. J. 146 (2009) 345–354.

[21] D. Kumar, J.P. Gaur, Chemical reaction- and particle diffusion-based kinetic modeling of metal biosorption by a Phormidium sp.-dominated cyanobacterial mat, Bioresour. Technol. 102 (2011) 633–640.
[22] F.C. Wu, R.L. Tseng, R.S. Juang, Comparisons of porous and adsorption properties of carbons activated by steam and KOH, J. Colloid Interface Sci. 283 (2005) 49–56.
[23] K.V. Kumar, V. Ramamurthi, S. Sivanesan, Modeling the mechanism involved during the sorption of methylene blue onto fly ash, J. Colloid Interface Sci. 284 (2005) 14–21.
[24] L.L. Fan, C.N. Luo, X.J. Li, F.G. Lu, H.M. Qiu, M. Sun, Fabrication of novel magnetic chitosan grafted with graphene oxide to enhance adsorption properties for methyl blue, J. Hazard. Mater. 215–216 (2012) 272–279.
[25] M.J. Iqbal, M.N. Ashiq, Adsorption of dyes from aqueous solutions on activated charcoal, J. Hazard. Mater. 139 (2007) 57–66.
[26] T. Wu, X. Cai, S. Tan, H. Li, J. Liu, W.D. Yang, Adsorption characteristics of acrylonitrile, p-toluenesulfonic acid, 1-naphthalenesulfonic acid and methyl blue on graphene in aqueous solutions, Chem. Eng. J. 173 (2011) 144–149.
[27] M. Mahramanlioglu, I. Kizilcikli, I.O. Bicer, Adsorption of fluoride from aqueous solution by acid treated spent bleaching earth, J. Fluorine Chem. 115 (2002) 41–47.